FISEVIER

#### Contents lists available at ScienceDirect

# Thin Solid Films

journal homepage: www.elsevier.com/locate/tsf



# The resistivity–temperature behavior of Al<sub>x</sub>CoCrFeNi high-entropy alloy films



Chenyu Wang<sup>a</sup>, Xiaona Li<sup>a,\*</sup>, Zhumin Li<sup>a</sup>, Qing Wang<sup>b,\*\*</sup>, Yuehong Zheng<sup>c</sup>, Yue Ma<sup>b</sup>, Linxia Bi<sup>a</sup>, Yuanyuan Zhang<sup>b</sup>, Xihui Yuan<sup>b</sup>, Xin Zhang<sup>b</sup>, Chuang Dong<sup>a</sup>, Peter K. Liaw<sup>d</sup>

- a Key Laboratory of Materials Modification by Laser, Ion and Electron Beams (Ministry of Education), Dalian University of Technology, Dalian 116024, China
- b School of Materials Science and Engineering, Dalian University of Technology, Dalian 116024, China
- c State Key Laboratory of Advanced Processing and Recycling of Nonferrous Metals, Lanzhou University of Technology, Lanzhou 730050, China
- <sup>d</sup> Department of Materials Science and Engineering, University of Tennessee, Knoxville, TN 37996, USA

#### ARTICLE INFO

#### Keywords: High-entropy alloy Thin-film resistors Resistivity–temperature behavior Disordered solid-solutions

#### ABSTRACT

Comprehensive understandings for the resistivity – temperature behavior of high-entropy alloy (HEA) films is crucial for assessing their potential as thin-film resistive materials. But due to the great difference between the structure of bulk and film materials, the resistivity – temperature behavior of the bulk HEAs cannot be directly introduced to understand the evolution law of the resistivity of HEA films with temperature. The present work investigated the resistivity change with temperature from room temperature to 1078 K of Al<sub>x</sub>CoCrFeNi (x=0.7,1.0) HEA films composed of face- and body-centered-cubic phases, and compared it with that of bulk HEAs with similar compositions. It was found that the Al<sub>x</sub>CoCrFeNi HEA films exhibit the ultralow temperature coefficient of resistance (TCR) within a range of  $\pm$  10 ppm/K, and their resistivity is tunable over a wide range from 191.8  $\mu\Omega$ ·cm (x=1.0) to 535.9  $\mu\Omega$ ·cm (x=0.7), which is beyond the reach of conventional alloy films. For both the film and bulk Al<sub>x</sub>CoCrFeNi HEAs, the resistivity – temperature behaviors exhibit similar characteristics of high resistivity and low TCRs before phase transitions, and can be described by the equation,  $\rho=b_0+b_1T(1-b_2T^2)$ , with the consideration of the phonon scattering and the s-d scattering effect in transition metals. The multi-principal element mixing feature of HEAs will open up more approaches to optimize the properties of thin-film resistive materials.

#### 1. Introduction

With the rapid development of the info-communication, aerospace, and precision measurement industries, the requirements are becoming more rigorous for electronic components in terms of accuracy, reliability, and integration. Thin-film resistors as basic electronic components also face an increasing demand. The thin-film resistive materials generally exhibit high resistivity accuracy and a small temperature coefficient of resistance (TCR) (i.e., good temperature stability). Furthermore, a wide range of tunable resistivity and higher application temperatures are also being pursued [1–4]. Disordered concentrated solid-solution alloys with solutes greater than 5 at.% (atomic percent) [5] are preferred for thin-film resistive materials owing to their high resistivity ( $\sim 10^2 \ \mu\Omega \cdot cm$ ), low TCRs (within  $\pm 10^3 \ ppm/K$ ) [6], and large ranges of application temperature (the highest disorder–order transition temperature can be up to 573 K [7]). The most typical

disordered concentrated alloys are alloys containing transition metals [6]. However, the resistivity ranges are relatively limited for alloys composed of transition metal elements alone. Currently, their nitrides, oxides, and silicides are used to substantially improve the resistivity, but the cost and complexity of the preparation process are also increased [8–11]. Therefore, one of the key problems is to find an excellent performance and economic disordered concentrated alloy.

High-entropy alloys (HEAs) which have been widely explored in recent years generally possess simple solid-solution structures, and thus are also regarded as solid-solution alloys with extremely high concentrations and complexity [5, 12–14]. From this viewpoint, HEAs should have giant potentials in the applications as thin-film resistive materials. However, literatures on the resistivity–temperature behavior of HEAs have mainly focused on bulk alloys, and have already proved that the bulk HEAs have relatively-high resistivity and low TCRs [15–19]. For instance, the most studied  $Al_x$ CoCrFeNi (0  $\leq x \leq$  2) HEAs

E-mail addresses: lixiaona@dlut.edu.cn (X. Li), wangq@dlut.edu.cn (Q. Wang).

<sup>\*</sup> Corresponding authors.

<sup>\*\*</sup> Corresponding authors.

have room temperature (RT) resistivity ranges between 90 and 200  $\mu\Omega$ -cm; meanwhile, the resistivity increases slowly with temperature as well as exhibits a nearly-linear manner from 4 to 400 K with TCRs in the range of 10–10³ ppm/K [15,16]. For the HEAs, the severe lattice distortion caused by the atoms random distribution is considered to be the main reason for the high resistivity. Namely, the atoms randomly occupy at the lattice sites, which causes asymmetric surroundings for each atom and the differences in size and bond energy between different neighboring atoms, eventually results in atoms deviation from the lattice sites at different positions. Thus the strong scattering of electrons by lattice distortion inevitably lead to high resistivity [20].

Shafeie et al. [19] studied the resistivity-temperature behavior of bulk Al<sub>x</sub>CoCrFeNi ( $1 \le x \le 3$ ) HEAs from 5 to 1200 K, established the strong correlation of the ultralow TCR with the underlying microstructure and local composition, and indicated that the negative TCRs are strongly related to the particle-size distribution and the Kondo temperatures. However, the grain sizes of the Al<sub>x</sub>CoCrFeNi HEA films are generally small due to the constraint of preparation methods. For instance, the width of columnar grains in the films prepared by magnetron sputtering are only of several tens nanometers since the film deposition can be considered as an instantaneous cooling process [21]. Therefore, the spinodal decomposition and the coherent precipitation occurred in the bulk Al<sub>x</sub>CoCrFeNi HEAs are not observed in the HEA films, and the results of bulk HEAs cannot be directly used to explain the resistivity-temperature behavior of HEA films. However, for the application prospect of HEAs as thin film resistors, it is necessary to understand not only the source of electrical resistance in the films, but also the resistivity-temperature behavior.

Currently, only a few reports [22–25] are available related to the resistivity–temperature behavior of HEA films. For the crystalline-phase  ${\rm Al}_x{\rm CoCrCuFeNiTi}_y$  HEA films [22], the resistivity was measured from RT to 573 K for two cycles. The TCRs (~1000 ppm/K) were only calculated in the second cycle, and the sharp resistivity decline with increasing temperature in the first cycle causing by whether the ordering or phase transitions was not discussed. For the amorphous BNbTaTiZr HEA film [23], the negative TCRs observed over the whole temperature range (225–400 K) was believed caused by the thermal expansion and activation effects. While the TCR study of the amorphous AlCrNiSiTa and NiCrMnYNb $_x$  HEA films [24,25] measured by the ex-situ method showed that the TCR shifted from negative to close to zero, which was attributed to crystalline and oxidation.

Magnetron sputtering has attracted more attention since this technique could prepare many species of thin films including refractory alloy films and composite films, which is an important thin film deposition technology in industry applications due to its good film-forming ability, high efficiency, low substrate temperature and good film adhesion. In particular, magnetron sputtering can ensure the films composition homogeneity; meanwhile, the films stoichiometry can be easily controlled by varying the chemical composition of a given target and the process parameters during sputtering [26], which made it become an optimal choice for the preparation of multi-component alloy films. For instance, Feng et al. [27] prepared a series of Al<sub>x</sub>CoCrFeNi HEA films on the Si substrate by direct current (DC) magnetron sputtering and found that extremely thin nanotwins induced by plastic deformation can enhance their strain rate sensitivity, although softening the films. In Liao's work [28,29], the Al<sub>x</sub>CoCrFeNi HEA films on

the Si substrate with different thickness were prepared by radio frequency (RF) magnetron sputtering. The high hardness of the films is ascribed to the formation of nanocrystal structure inside the thin films and the preferred growth orientation.

In summary, in the present paper, the  ${\rm Al}_x{\rm CoCrFeNi}$  HEA films (x=0.7 and 1.0) will be prepared by magnetron sputtering and the resistivity evolution from RT to 1078 K will also be studied. Then the resistivity–temperature behavior of the HEA films will be compared to that of bulk HEAs with similar compositions. Finally, the source of resistance in the HEA films and the mechanism of resistivity evolution with temperature will be analyzed. The research will not only contribute to a more comprehensive understanding of the essential properties of HEA films, but also of great significance for expanding their applications.

#### 2. Experimentals

#### 2.1. Materials preparation

Three Al<sub>x</sub>CoCrFeNi HEA films were deposited on the single-crystal Si (100) substrates using a JGP450 magnetron-sputtering system. All the as-deposited films show high brightness (The films have high reflectivity. The reflectivity of the Al<sub>0.6</sub>CoCrFeNi HEA film is within the range of 35-55% from visible to near-infrared band) and good adhesion. The sputtering target with the diameter of 75 mm was prepared by arc-melting with fixed composition a  $\text{Al}_{12.5}\text{Co}_{21.875}\text{Cr}_{21.875}\text{Fe}_{21.875}\text{Ni}_{21.875}$  unit in at.%, and the purity of each component was no less than 99.9 at.%. The substrate rotated in a constant speed of 10 r/min., and the working distance was about 10 cm. The base pressure of the chamber was lower than  $4.0 \times 10^{-4}$  Pa before pure Argon was added. The flow rate of the Argon was set at 10.0 standard cubic centimeters per minute (sccm) to keep the working pressure at around 1.40 Pa. The temperature of the substrate raised not exceeding 50 °C during the sputtering process.

The sputtering parameters for each film were listed in Table 1. Power supplies (radio frequency (RF) or direct currents (DC)) and time were adjusted for each sputtering process, and the power remained at 100 W. An RF power supply was used for the 30 and 90 min. sputtering, whereas a DC power supply for the 60 min. sputtering. Table 1 also gives the film compositions measured by the electron probe microanalyzer (EPMA-1600, Kyoto, Japan), as well as the film thicknesses (measured by a profilometer (ET4000M, Kosaka, Japan)). It can be seen that the film compositions and thicknesses change with the sputtering parameters, whereas the differences between the actual film compositions and that of the sputtering target are mainly due to different sputtering thresholds and rates among these elements. The film compositions were used to calculate the molar proportions of the three films, which are approximately as AlCoCrFeNi, Al<sub>0.7</sub>CoCrFeNi, and Al<sub>0.7</sub>CoCrFeNi, respectively. Since the latter two are too close to be differentiated, different types of power supplies were added to the molar proportions as a distinction, as shown in Table 1, which are referred to as "AlCoCrFeNi<sub>RF</sub>, Al<sub>0.7</sub>CoCrFeNi<sub>DC</sub>, and Al<sub>0.7</sub>CoCrFeNi<sub>RF</sub>".

The two bulk  $Al_x$ CoCrFeNi HEAs were synthesized by arc melting. The raw elemental metals Al, Co, Fe, and Ni had the purity of 99.99 at. % and Cr of 99.9 at.%. Alloy ingots were re-melted at least four times to ensure chemical homogeneity, and then were copper-mold suction-

Table 1
Sputtering parameters, thicknesses, and compositions of the Al<sub>x</sub>CoCrFeNi HEA films.

Sputtering parameters Power supply	Time (min)	Power (W)	Thickness (nm)	Composition (at.%)	Molar proportion
radio frequency	30	100	205	Al <sub>20.85</sub> Co <sub>21.21</sub> Cr <sub>18.89</sub> Fe <sub>18.38</sub> Ni <sub>20.67</sub>	$AlCoCrFeNi_{RF}$
direct current	60	100	520	$Al_{14.44}Co_{21.97}Cr_{20.28}Fe_{20.54}Ni_{22.77}$	Al <sub>0.7</sub> CoCrFeNi <sub>DC</sub>
radio frequency	90	100	570	$\mathrm{Al}_{14.25}\mathrm{Co}_{22.74}\mathrm{Cr}_{21.45}\mathrm{Fe}_{19.81}\mathrm{Ni}_{21.75}$	${\rm Al}_{\rm 0.7}{\rm CoCrFeNi}_{\rm RF}$

casted into cylindrical rods with a diameter of 6 mm. The mass loss during the preparation process was less than 0.1%. The compositions (at.%) of the two bulk HEAs are  $Al_{15.63}Co_{21.09}Cr_{21.09}Fe_{21.09}Ni_{21.09}$  and  $Al_{18.75}Co_{20.31}Cr_{20.31}Fe_{20.31}Ni_{20.31}$ , which are referred to as "Bulk-Al<sub>0.74</sub>CoCrFeNi, and Bulk-Al<sub>0.92</sub>CoCrFeNi", also by their respective molar proportions.

#### 2.2. Characterization

The structures of the films and bulk alloys were analyzed using two different x-ray diffractometers (XRD, Bruker D8 Discover, the grazing incidence mode with an incident angle of 1°; Bruker D8 Focus, the  $\theta$ –2 $\theta$ mode, Karlsruhe, Germany). To perform the microstructural characterization for the films, both the in-plane and cross-sectional thin-foil specimens of the films (wedge-shaped, thickness on one side was less than 5 µm) were prepared by mechanical milling, and then were thinned by ion milling at RT to about 30 nm. The prepared specimens were observed by a transmission electron microscope (TEM, JEOLJEM-ARM200F, 200 kV, Kyoto, Japan). The high-resolution (HR) and scanning transmission electron microscopy (STEM) imaging were conducted, and the in situ energy-dispersive x-ray spectroscopy (EDS) of the TEM was used for analyzing the elemental distributions. The hardness of the films were measured by a nano-indenter (MTS XP, Berkovich indenter, Minnesota, USA), and the same strain rate was maintained for all loading processes. A four-point probe tester (RTS-9, Guangzhou, China) was employed to obtain the RT resistivity of the films. The resistivity-temperature measurements were carried out with a thermal resistance tester (TRT-1000, Wuhan, China). The films and bulk alloys were heated from RT to 1078 K with a constant heating rate of 10 K/min., and then were cooled with the furnace in vacuum to RT.

#### 3. Results

## 3.1. Microstructural characterization of film and bulk HEAs

Fig. 1 presents the XRD patterns of the film and bulk  $Al_x$ CoCrFeNi HEAs. The Bulk- $Al_{0.74}$ CoCrFeNi alloy is mainly composed of the bodycentered-cubic (BCC) and B2 phases, and contains a small amount of the face-centered-cubic (FCC) phase, whereas the Bulk- $Al_{0.92}$ CoCrFeNi

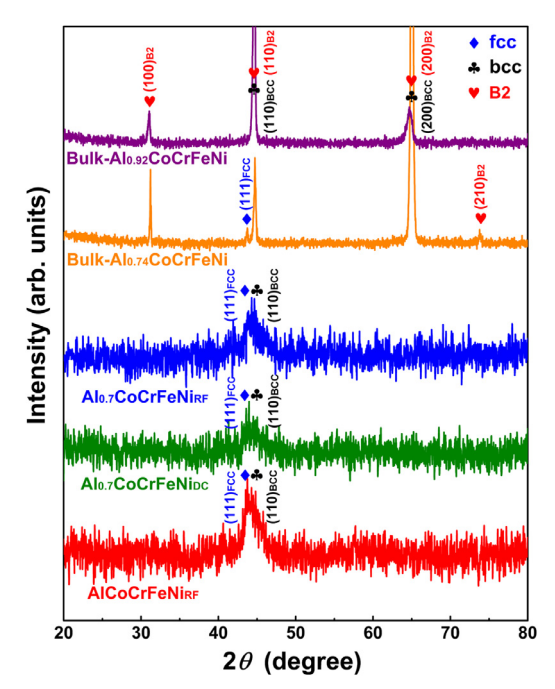


Fig. 1. XRD patterns of the film and bulk Al<sub>x</sub>CoCrFeNi HEAs.

alloy is only composed of the BCC and B2 phases. However, the films only present one wide diffraction peak at around 44°, causing it unable to determine the phase constitution. Further analysis combining the TEM results is necessary and the results show that the three films exhibit consistent characteristics, the uniform thickness, and the smooth and clear film-substrate interface. Fig. 2(a) presents the in-plane bright-field image with the corresponding selected-area electron diffraction (SAED) pattern of the AlCoCrFeNi<sub>RF</sub> film. The film exhibits good crystallization and is composed of columnar grains with the diameter around 20 nm. The SAED pattern shows that the films are composed of the FCC and BCC phases. The HRTEM images for investigating nanocrystals in the Al<sub>0.7</sub>CoCrFeNi<sub>DC</sub> film are displayed in Fig. 2(b). Only the FCC and BCC phases were found after analyzing the fast Fourier transform (FFT) spectra in multiple areas, further confirming the structures of these HEA films. Fig. 2(c) presents a dark-field crosssectional STEM image of the Al<sub>0.7</sub>CoCrFeNi<sub>DC</sub> film, along with the EDS mappings of each element in the same area. The element Al, Co, Cr, Fe, and Ni distribute randomly in the film, which agrees well with the chemical disorder of HEAs.

Since the transition of FCC  $\rightarrow$  BCC  $\rightarrow$  B2 in the Al<sub>x</sub>CoCrFeNi HEAs is essentially a process of ordering [30–36]. Thus, the abovementioned Al<sub>x</sub>CoCrFeNi HEA films with the FCC and BCC phases are more disordered than the bulk HEAs consisted mainly of the BCC and B2 phases. Crystalline structures of film and bulk alloys can be very different even with similar compositions owing to the preparation methods. In theory, film deposition can be considered as an extremely-rapid quenching process; that is, instantaneous cooling from a temperature at or above the melting point of the alloy to the substrate temperature [21]. Therefore, the Al<sub>x</sub>CoCrFeNi films did not have enough time to undergo the disorder–order transition.

#### 3.2. Hardness and elastic-modulus analysis

Fig. 3 displays the load–displacement curves of the  ${\rm Al_xCoCrFeNi}$  HEA films with different indentation depths, in which the maximum displacement for the  ${\rm AlCoCrFeNi}_{\rm RF}$  film is 200 nm considering its thickness (205 nm), and those for the other two films are 300 nm. For each film, the loading parts of the curves with different maximum displacements all show good repeatability, indicating the excellent uniformity of these films. The 100 nm curves with the minimal substrate interference were selected to compare the loading processes of the three films. As presented in the enlarged graph at the top left of Fig. 3, the loading part of the  ${\rm Al_{0.7}CoCrFeNi_{DC}}$  film stayed at the lowest throughout the whole process, which means that its hardness and elastic modulus are the smallest among three. The loading parts of the  ${\rm AlCoCrFeNi_{RF}}$  and  ${\rm Al_{0.7}CoCrFeNi_{RF}}$  films almost overlapped at first, but then the latter gradually exceeded the former as the displacement increased.

Fig. 4(a) and (b) present the hardness- and modulus-displacement curves of the HEA films, respectively. To avoid the substrate interference, the hardness and modulus of each film were obtained at the displacement where equals 1/7th of the thickness. The hardness (10.25  $\pm$  0.74 GPa) and modulus (208  $\pm$  9.7 GPa) of the Al<sub>0.7</sub>CoCrFeNi<sub>RF</sub> film are the highest among the three films, whereas the  $Al_{0.7}$ CoCrFeNi<sub>DC</sub> film has the lowest hardness (7.13  $\pm$  0.79 GPa) and modulus (181  $\pm$  11.2 GPa), although these two films have very similar compositions and thicknesses. This behavior can be explained by the growth rate of the films calculated from the sputtering time and thickness. The growth rate of the Al<sub>0.7</sub>CoCrFeNi<sub>DC</sub> film is 8.7 nm/min., and those of the AlCoCrFeNi<sub>RF</sub> and Al<sub>0.7</sub>CoCrFeNi<sub>RF</sub> film are 6.8 nm/ min. and 6.3 nm/min., respectively. It is obvious that the Al<sub>0.7</sub>CoCrFeNi<sub>DC</sub> film grew much faster than the other two films, which leads to its relatively-loose structure, and thus explains its minimum hardness and modulus. The differences between the growth rates of these films are mainly attributed to the sputtering power supplies (DC and RF). Judging from the results, although DC magnetron sputtering

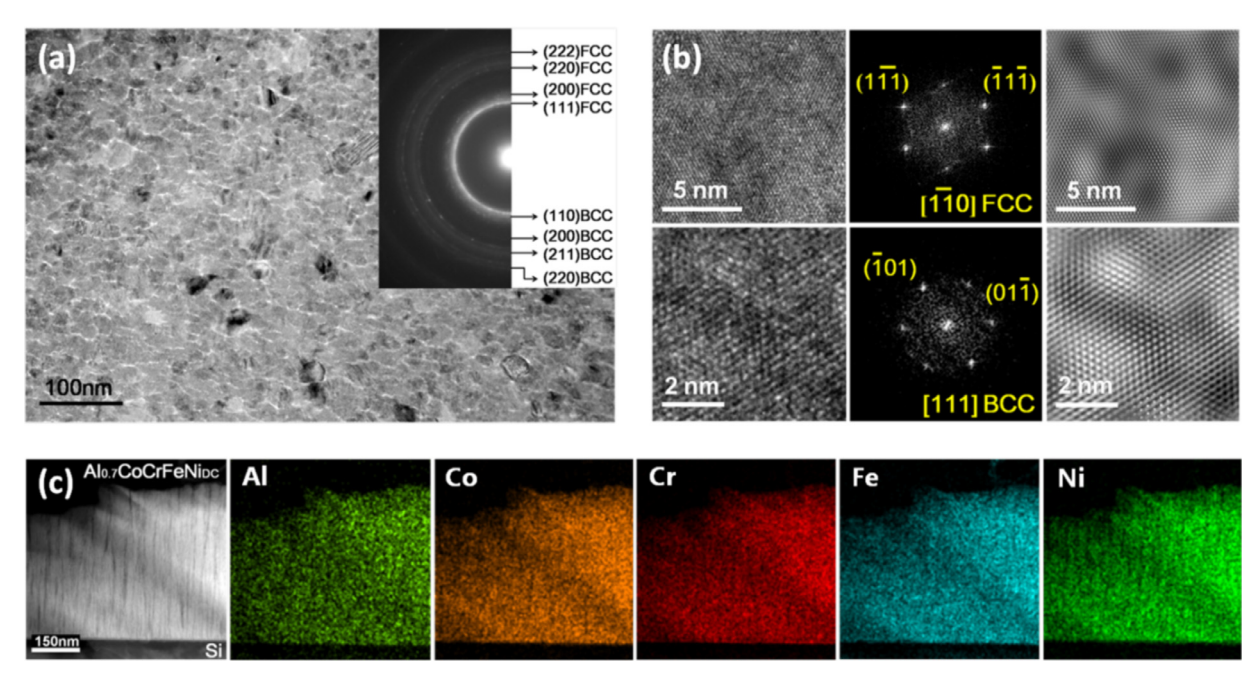
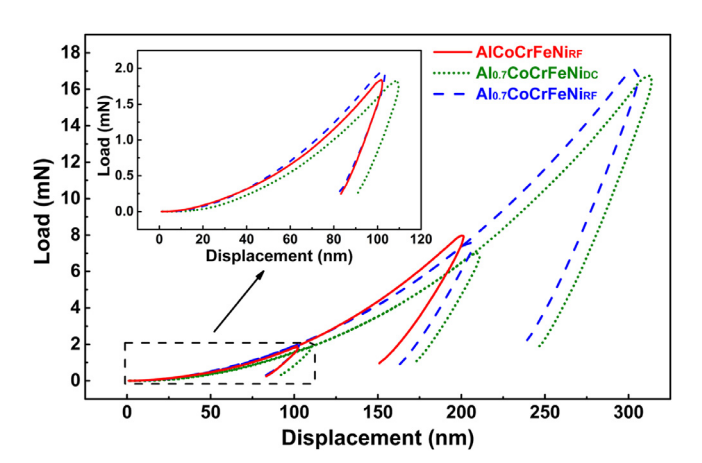


Fig. 2. Microstructures of the  $Al_x$ CoCrFeNi HEA films. (a) The bright-field in-plane TEM morphology of the  $Al_{CO}$ CrFeNi $_{RF}$  film and the corresponding SAED pattern. (b) The HR images, the corresponding FFT spectra and filtered HR images of the FCC and BCC structures in the  $Al_{0.7}$ CoCrFeNi $_{DC}$  film. (c) The dark-field cross-sectional STEM morphology of the  $Al_{0.7}$ CoCrFeNi $_{DC}$  film and the EDS mappings of each element in the same area.



**Fig. 3.** Load – displacement curves of the  ${\rm Al_xCoCrFeNi}$  HEA films. The maximum displacement of the  ${\rm AlCoCrFeNi}_{\rm RF}$  film is 200 nm considering its thickness (205 nm), and those of the other two films are 300 nm. The enlarged graph of the 100 nm curves of the three films is displayed at the top left of this figure.

also is a successful coating technique, it suffers from fundamental problems, such as low target utilization and target poisoning during reactive sputtering, which results in process instabilities and poor deposition rates [37]. In comparison, RFmagnetron sputtering is advantageous to obtain  ${\rm Al}_x{\rm CoCrFeNi}$  HEA films with higher hardness and moduli. In the comparative study of  ${\rm Al}_2{\rm O}_3$  films, Cremer et al. [38] founded that the hardness of DC sputtered films is significantly lower than that of the RF sputtered films. In the works of Tan et al. on the  ${\rm CrN}_x$  films, similar behavior of hardness between DC and RF sputtered films was also observed, which was believed mainly due to the distinct difference between the dense structure (RF process) and the porous structure (DC process) [39].

The formation of the B2-phase precipitates is the main reason for the high-temperature aging hardening of  $Al_xCoCrFeNi$  HEAs. For example, in an  $Al_{0.3}CoCrFeNi$  alloy, a large amount of B2-phase precipitates formed after the heat treatment at 973 K for 24 h, resulting in a 65% increase of the hardness, compared with that of the as-cast state [40]. At room temperature, the hardness of the bulk  $Al_xCoCrFeNi$  HEAs

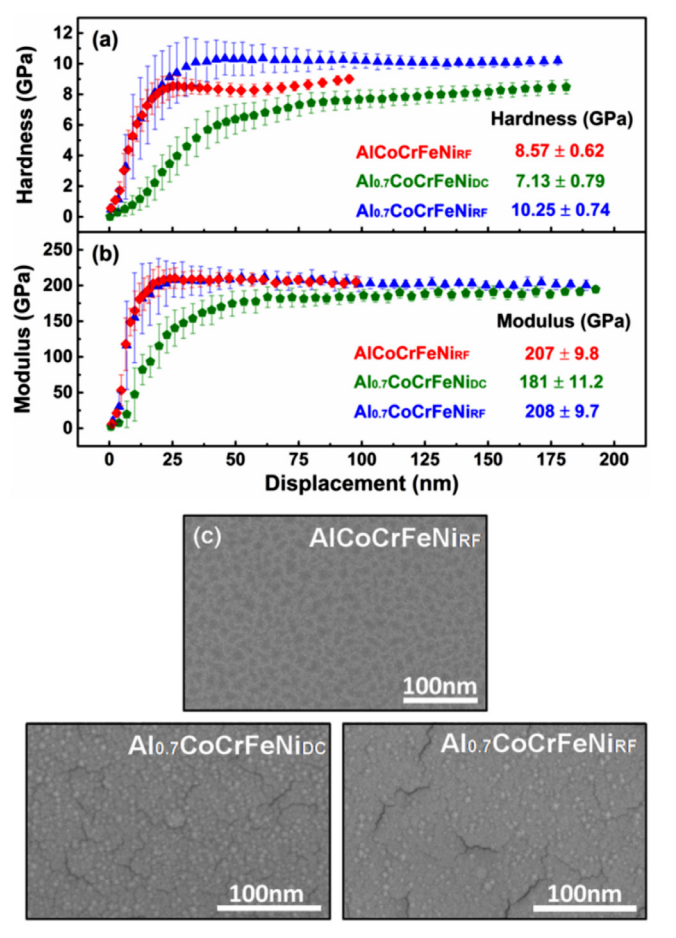


**Fig. 4.** The hardness, elastic modulus, and SEM surface morphologies of the Al<sub>x</sub>CoCrFeNi HEA films. (a) The hardness—displacement curves. (b) The modulus—displacement curves. The hardness and modulus of each film were obtained at the displacement which equals 1/7th of the thickness. (c) The SEM secondary-electron images of the in-plane surface morphologies.

generally increases with the Al content, which is also caused by the increase of the amounts of the hardening BCC and B2 phases. For instance, the as-cast bulk  $Al_x$ CoCrFeNi alloys (x = 0.5 and 0.75) are both consisted of the FCC and BCC phases. However, as the Al content increased, the Al<sub>0.75</sub>CoCrFeNi alloy has a larger amount of the BCC phase, resulting in its Vickers hardness more than 200 kgf/mm<sup>2</sup> higher than that of the Al<sub>0.5</sub>CoCrFeNi alloy [30]. However, comparing the film and bulk Al<sub>x</sub>CoCrFeNi HEAs in this paper, the HEA films have the hardness in the range between 7.13  $\pm$  0.79 to 10.25  $\pm$  0.74 GPa. The hardness of the Bulk-Al $_{0.74}$ CoCrFeNi alloy is 5.18  $\pm$  0.11 GPa, and that of the Bulk-Al<sub>0.92</sub>CoCrFeNi alloy is 5.20  $\pm$  0.09 GPa. Although the bulk HEAs contain higher amounts of the hardening BCC and B2 phases than the HEA films, their hardness is still much lower, which is because the HEA films are composed of nanocrystals. Another trend worth mentioning is that the Al<sub>0.7</sub>CoCrFeNi<sub>RF</sub> film with a lower Al content has higher hardness than the AlCoCrFeNi<sub>RF</sub> film, which exhibits an opposite behavior, compared with the bulk HEAs mentioned in the literature [30] above. This trend indicates that apart from the Al content, the film hardness is also affected by multiple complex factors, such as the thickness and internal stress.

**Fig. 4(c)** displays the SEM secondary-electron images of the inplane surface morphologies of the Al<sub>x</sub>CoCrFeNi HEA films. The surface of the AlCoCrFeNi<sub>RF</sub> film is relatively uniform and consistent, whereas many scattered microcracks appear on the surface of the Al<sub>0.7</sub>CoCrFeNi<sub>DC</sub> and Al<sub>0.7</sub>CoCrFeNi<sub>RF</sub> films. The formation of microcracks on these two films is mainly attributed to the relatively-high internal stress caused by the larger thickness (more than 200 nm thicker than the AlCoCrFeNi<sub>RF</sub> film). Compared with those in the Al<sub>0.7</sub>CoCrFeNi<sub>DC</sub> film, the microcracks in the Al<sub>0.7</sub>CoCrFeNi<sub>RF</sub> film are larger, which indicates that the Al<sub>0.7</sub>CoCrFeNi<sub>RF</sub> film has even the higher internal stress than that of the Al<sub>0.7</sub>CoCrFeNi<sub>DC</sub> film. Overall, among the three films, the Al<sub>0.7</sub>CoCrFeNi<sub>RF</sub> film possesses the relatively-compact structure and high internal stresses, which will obviously leads to its highest hardness.

#### 3.3. The resistivity-temperature behavior

The resistivity–temperature curves of the  ${\rm Al_xCoCrFeNi}$  HEA films are presented in Fig. 5. Depending on the variation range of resistivity, the curves can be divided into two stages. From RT to 565 K, where resistivity changed very little with temperature, especially for the two films prepared by the RFmagnetron sputtering, their resistivity almost remained constant, whereas the resistivity of the  ${\rm Al_{0.7}CoCrFeNi_{DC}}$  film showed a slight upward then downward trend. Therefore, if considering the stability of resistivity, the HEA films prepared by the RF magnetron

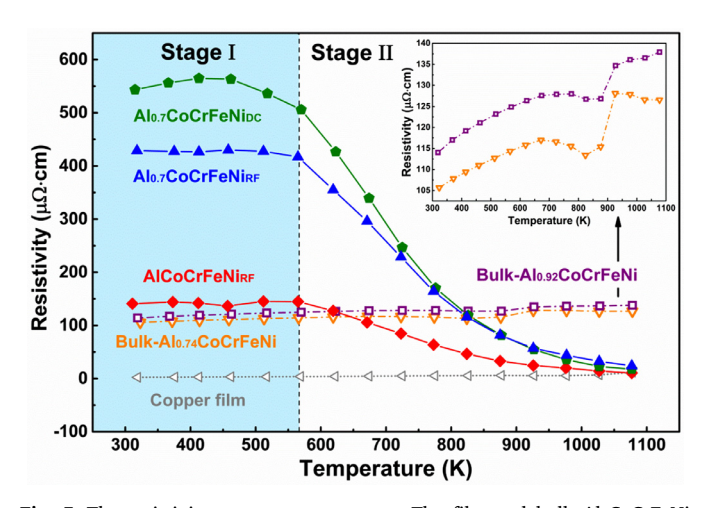


Fig. 5. The resistivity—temperature curves. The film and bulk  ${\rm Al_xCoCrFeNi}$  HEAs and a copper film for comparison are included. A magnified view of the curves of bulk HEAs is displayed at the top right of this figure.

sputtering displayed the better performance than that prepared by the DC magnetron sputtering. In the second stage from 565 K to 1078 K, the resistivity of the three films started to drop at almost the same temperature around 565 K and decreased dramatically, and then eventually reached near the same value of 20 μΩ·cm at 1078 K. The resistivity of the Al<sub>0.7</sub>CoCrFeNi<sub>DC</sub> film displayed the largest decrease, dropping from 505.9 at 565 K to 81.4  $\mu\Omega$ ·cm at 873 K. To exclude the possibility that the resistivity decrease of the HEA films is caused by the growth and aggregation of crystal grains, the resistivity change of a nanocrystalline copper film prepared by magnetron sputtering was also measured in the same condition and displayed in Fig. 5 for comparison. Unlike the HEA films, the resistivity of the copper film increased slowly within the whole temperature range, indicating that the decrease of the resistivity caused by the grain growth during heating did not dominate the resistivity-temperature behavior of the films. In addition, diffusions in HEAs can be much slower than that in pure metals [13]. Therefore, the resistivity decrease of the HEA films is even more unlikely to be caused by the grain growth.

For the resistivity–temperature curves of the two bulk  ${\rm Al_xCoCrFeNi}$  HEAs, as also shown in Fig. 5, their resistivity slowly increased from RT to 1078 K, which is obviously different from the behavior of the HEA films. On closer inspection, as shown in the magnified view of the curves of bulk HEAs at the top right of Fig. 5, the resistivity maintained a stable increasing trend until about 723 K when disturbances appeared and the curves deviate from their original trend. Then at around 873 K, a sudden small increase appeared.

#### 4. Discussion

#### 4.1. The first stage of resistivity-temperature behavior

#### 1) TCRs of the film and bulk Al<sub>x</sub>CoCrFeNi HEAs

According to Fig. 5, in the first stage where resistivity maintained the initial trend and changed slowly, that is, from RT to 565 K and to 723 K for the film and bulk  $Al_x$ CoCrFeNi HEAs, respectively, TCRs of the film and bulk  $Al_x$ CoCrFeNi HEAs are calculated by the following formula:

$$TCR = \frac{(\rho_T - \rho_R)}{\rho_R (T - T_R)} \tag{1}$$

where  $\rho_R$  and  $\rho_T$  are the resistivity at RT and at another temperature, respectively. For the Al $_x$ CoCrFeNi HEA films, from RT to 565 K, the TCRs fluctuate in a small range and near zero (–27 to 36 ppm/K), especially the Al $_0.7$ CoCrFeNi $_{RF}$  film (–10 to 2 ppm/K). For the bulk Al $_x$ CoCrFeNi HEAs, the Bulk-Al $_0.74$ CoCrFeNi and Bulk-Al $_0.92$ CoCrFeNi alloys have small positive TCRs range between 25 and 55 ppm/K from RT to 723 K

Based on the conductivity study of concentrated disordered alloys (such as NiCr alloys), an important conclusion had been drawn by Mooij [6] that these alloys generally possess large resistivity and small or even negative TCRs. More importantly, at least one transition metal element is contained, and the crystal structure of the alloys has little influence on their resistivity–temperature behavior. The correlation between high resistivity and small TCRs is in accord with the saturation effect in the electron transport, and this effect had already been explained by Cote and Meisel [41,42]. When considering the electron—phonon interactions, phonons with wavelengths exceeding the electron mean free path can be regarded as ineffective electron scatterers, namely, there exists a limiting resistivity when the electron mean free path approaches the interatomic spacing. For both crystalline and amorphous alloys, the resistivity ( $\rho$ ) can be expressed by the equation [42]:

$$\rho = (1 - \gamma)\rho_{ip} + \rho_0 e^{-2W^*} \tag{2}$$

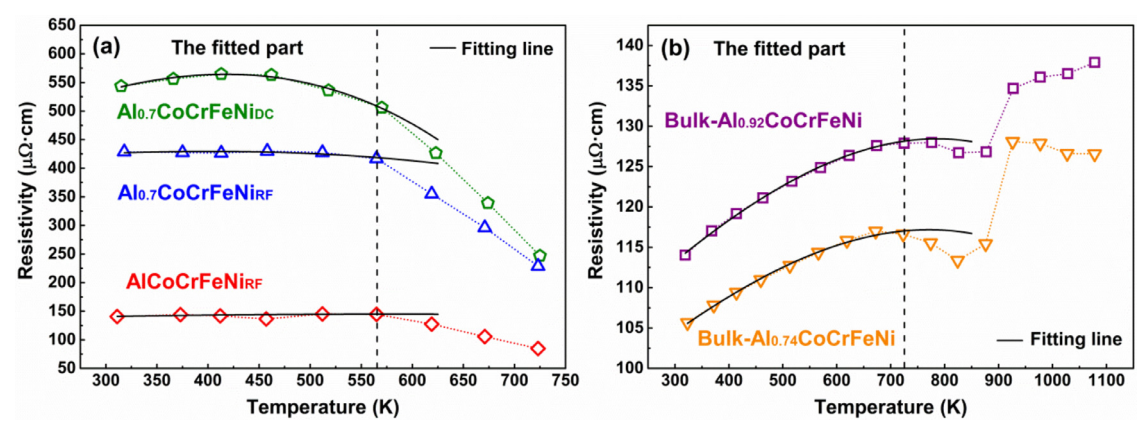


Fig. 6. The resistivity – temperature curves fitted by the equation,  $ρ = b_0 + b_1T(1 - b_2T^2)$ . (a) The fitted curves of the Al<sub>x</sub>CoCrFeNi HEA films from RT to 565 K. (b) The fitted curves of bulk Al<sub>x</sub>CoCrFeNi HEAs from RT to 723 K.

**Table 2** The fitted values of parameters,  $b_0$ ,  $b_1$ , and  $b_2$ , in the equation,  $\rho = b_0 + b_1 T(1 - b_2 T^2)$ .

Sample	$b_0$	$b_1$	$b_2$
AlCoCrFeNi <sub>RF</sub>	$130.668 \pm 12.918$	$0.037 \pm 0.005$	$9.997 \times 10^{-7} \pm 8.433 \times 10^{-8}$
Al <sub>0.7</sub> CoCrFeNi <sub>DC</sub>	$300.270 \pm 26.802$	$0.949 \pm 0.093$	$1.913 \times 10^{-6} \pm 3.916 \times 10^{-8}$
Al <sub>0.7</sub> CoCrFeNi <sub>RF</sub>	$390.624 \pm 26.596$	$0.144 \pm 0.092$	$2.056 \times 10^{-6} \pm 3.255 \times 10^{-7}$
Bulk-Al <sub>0.74</sub> CoCrFeNi	$88.787 \pm 1.271$	$0.055 \pm 0.004$	$5.605 \times 10^{-7} \pm 4.218 \times 10^{-8}$
Bulk-Al <sub>0.92</sub> CoCrFeNi	$95.059 \pm 0.956$	$0.064 \pm 0.003$	$5.401 \times 10^{-7} \pm 3.582 \times 10^{-9}$

where  $(1 - \gamma)\rho_{ip}$  is the inelastic (phonon) scattering term,  $\gamma = 2\pi/\Lambda q_D$ ,  $\Lambda$  is the electron mean free path,  $q_D$  is the Debye wave vector, and  $ρ_{ip}$  is the ideal one-phonon resistivity ( $\Lambda \rightarrow \infty$ ).  $\rho_0 e^{-2W^*}$  is the elastic (structure) scattering term, where  $\rho_0$  is the residual resistivity at T = 0 K,  $e^{-2W^*}$  is the Debye-Waller factor with an averaged Debye-Waller exponent,  $2W^*$ . If the initial resistivity is large,  $\Lambda$  will be small and will lead to a large  $\gamma$ , indicating that the phonon scattering term  $(1 - \gamma)\rho_{ip}$  in Eq. (2) with a positive TCR will decrease. Small or even negative TCRs might occur when the initial resistivity is large enough. On the other hand, if the initial resistivity reaches its limit, according to Eq. (2), the term,  $(1 - \gamma)\rho_{ip}$ , no longer changes with temperature, and the effect of the Debye-Waller factor,  $e^{-2W^*}$ , on  $\rho_0$ becomes smaller as the temperature increases. That is, whether the resistivity is dominant by phonon or structure scattering, it is a common feature for high-resistivity alloys that the saturation effect exists; namely, their resistivity becomes essentially independent of temperature [42]. For the Al<sub>x</sub>CoCrFeNi HEAs, both the film and bulk alloys have the high RT resistivity (the initial resistivity). Therefore, their TCRs are no longer large positive values, but instead fluctuate in a small range  $(\pm 50 \text{ ppm/K})$  near zero.

#### 2) Reasons for the high initial resistivity

According to the model given by Mott and Jones [43], the resistance of a metal is originated from the scattering of electrons by phonons, impurities or defects, and other electrons. All factors that increase the scattering will lead to the raise of resistivity. There are two main reasons for the Al<sub>x</sub>CoCrFeNi HEAs having high initial resistivity (RT resistivity). One is the severe lattice distortion caused by chemical disorder; the strong scattering of electrons leads to the high resistivity. The other is the s-d scattering effect in transition metals.

The  ${\rm Al_x}$ CoCrFeNi HEAs contain four transition metal elements of Co, Cr, Fe, and Ni with the whole content higher than 80 at.%. Therefore, the structure of these alloys can be regarded as a transition-metal matrix with solutes of the non-transition metal (Al). Considering that Al has a relatively-large atomic radius, and there exist sluggish diffusion effects in HEAs [13], the resistivity caused by the Al solutes can be

approximately regarded as independent with temperature.

It is a characteristic for transition metals that the d band is unfilled, and the conductive electrons include those from the unfilled d band and the filled s band. The conductive s electrons will transfer to the d band after scattering, which will decrease the electron mean free path and therefore, increase the resistance [43]. This behavior (the s-d scattering effect) contributes to the relatively-high resistivity of transition metals, compared to noble or alkali metals.

There are also reasons for the  ${\rm Al_xCoCrFeNi}$  HEA films having higher resistivity than the bulk HEAs; that is, the HEA films are composed of nanocrystals and are more chemically disordered (proved in the microstructural characterization section).

If comparing the range of RT resistivity, for the bulk Al<sub>x</sub>CoCrFeNi HEAs, as the Al content increased by x = 0.18, the resistivity only changed about 10 μΩ·cm. However, the resistivity of Al<sub>x</sub>CoCrFeNi HEA films changed more than 400 μΩ·cm as the Al content increased by x = 0.3. The differences between them are due to the fact that the film resistivity is affected by multiple factors, such as the composition, phase constitution, thickness, and internal stress. For homogeneous bulk materials, resistivity is an intrinsic property that does not change with thickness. However, for the films deposited by physical vapor deposition such as magnetron sputtering, on the one hand, the nano columnarcrystals have relatively small sizes in the early stage of deposition, and can become slightly larger with the deposition time. Therefore, the resistivity will decrease slightly with the increase of film thickness. On the other hand, the sputtering thresholds and rates of these five elements of are different. The differences will gradually increase with the sputtering time (film thickness), thus causing the varying compositions of the films and lead to the change of resistivity. In our work, the difference of resistivity between AlCoCrFeNi and Al<sub>0.7</sub>CoCrFeNi films is influenced by the above reasons. However, the resistivity of the AlCoCrFeNi<sub>RF</sub> film with smaller thickness is far less than that of the Al<sub>0.7</sub>CoCrFeNi film. Therefore, the different compositions between these films caused by the change of film thickness is the main reason for their different resistivity. The resistivity of Al<sub>0.7</sub>CoCrFeNi<sub>DC</sub> film is higher than that of the Al<sub>0.7</sub>CoCrFeNi<sub>RF</sub> film although they have very similar compositions and thicknesses. This behavior is mainly due to

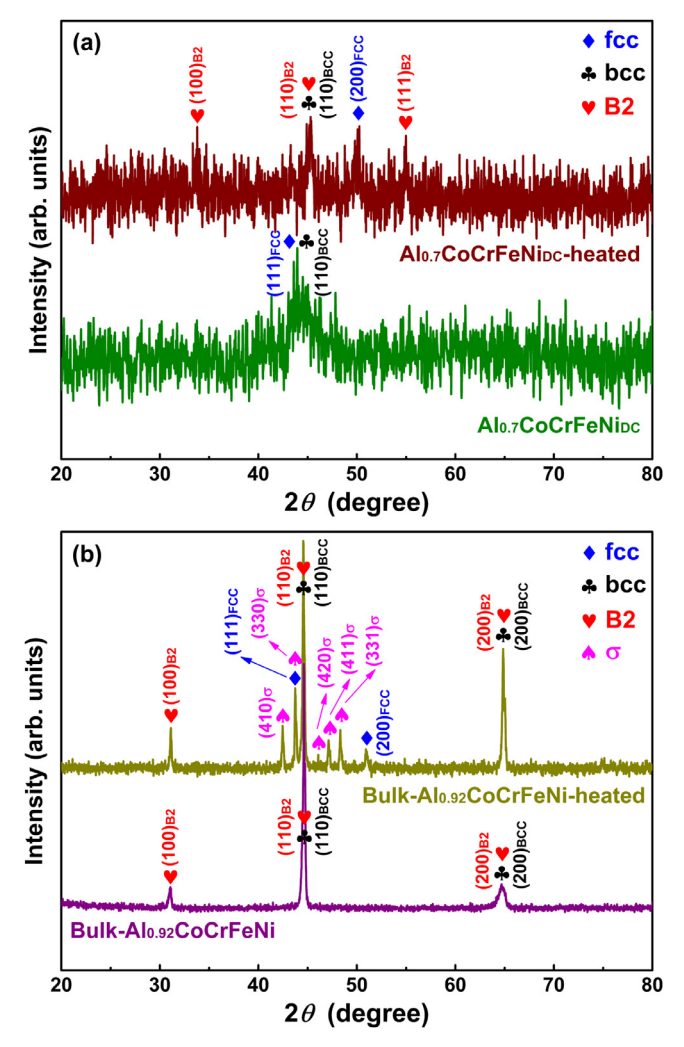


**Fig. 7.** Comparative XRD analysis before and after the resistivity – temperature measurements. (a) XRD patterns of the  $Al_{0.7}$ CoCrFeNi<sub>DC</sub> film. (b) XRD patterns of the Bulk- $Al_{0.92}$ CoCrFeNi alloy.

the fact that DC magnetron sputtering can induce more defects compared to RF magnetron sputtering [37]. Accordingly, the resistivity of the  ${\rm Al}_x{\rm CoCrFeNi}$  HEA films has a very expansive modulation space, and the multi-principal element mixing feature of HEAs is well reflected in this aspect.

#### 3) Descriptions of the resistivity-temperature behavior

For transition metals, the temperature dependence of the resistivity generated by the *s-d* scattering can be expressed as [43]:

$$\rho_{s-d}(T) \propto 1 - (\pi^2/6)(T/T_0)^2$$
(3)

where  $kT_0 = (E_0 - E_F)$ , k is the Boltzmann's constant,  $E_0$  and  $E_F$  are the Fermi energies of the d band at the temperatures of 0 K and T, respectively. It can be seen that  $\rho_{s-d}(T)$  decreases as the temperature increases.

In the  $Al_x$ CoCrFeNi HEAs, the resistivity due to electron – phonon scattering is proportional to T. The scattering of electrons by impurities or defects is approximately independent of temperature owing to the difficulties of diffusion caused by the lattice distortion in HEAs. Therefore, the resistivity of the  $Al_x$ CoCrFeNi HEAs changing with temperature can be described as:

$$\rho = b_0 + b_1 T (1 - b_2 T^2) \tag{4}$$

Eq. (4) can well fit the resistivity - temperature curves of film and

bulk  $Al_x$ CoCrFeNi HEAs in the first stage, as shown in Fig. 6(a) and (b). The fitting results confirm that the above analysis of the resistivity of the  $Al_x$ CoCrFeNi HEAs is correct, and the appearance of the small TCRs is also explained, which is consistent with the saturation effect. The fitted values of parameters in Eq. (4) are listed in Table 2. Coefficients  $b_1$  and  $b_2$  are relatively small, indicating the good temperature stability of the  $Al_x$ CoCrFeNi HEAs.

## 4.2. The second stage of resistivity - temperature behavior

To investigate the dramatic resistivity decrease of the HEA films at 565 K and the sudden small increase of the bulk HEAs at 873 K in Fig. 5, phase transitions need to be considered. The XRD patterns of the Al<sub>x</sub>CoCrFeNi HEAs before and after the resistivity – temperature measurements were compared. As shown in Fig. 7(a), the Al<sub>0.7</sub>CoCrFeNi<sub>DC</sub> film with the FCC and BCC phases developed the B2 phase after heating. In addition, the diffraction peak of the BCC phase shifted slightly to the right, and the orientation of the FCC phase adjusted to (200). Seen from Fig. 7(b), the diffraction peaks of the  $\sigma$  (P42/mnm, a=0.88 nm, c=0.45 nm) and FCC phases appeared after heating for the BCC- and B2-phases Bulk-Al<sub>0.92</sub>CoCrFeNi alloy. These results indicate that the BCC  $\rightarrow$  B2 transformation occurred in the HEA films during heating, whereas for the bulk HEAs, the main phase transition is BCC  $\rightarrow$   $\sigma$  + FCC.

Compared to the more close-packed FCC structure, the BCC structure is easier to diffuse when heated [33], which is the main reason why most transitions originate from the BCC phase. A schematic is depicted in Fig. 8 to illustrate the heat-induced BCC phase transitions in the Al<sub>x</sub>CoCrFeNi HEAs. The lattice-site positions of the disordered BCC phase are randomly occupied by atoms of the five elements with equal or nearly-equal probabilities, showing the high disordering. The BCC → B2 transformation takes place when Al atoms preferentially occupy the body-center position of the disordered BCC unit cells, which is essentially a process of ordering [36]. Since the lattice-distortion degree has strong effects on the resistivity of Al<sub>x</sub>CoCrFeNi HEAs, and it is mainly determined by the Al atoms due to the fact that the atomic radius of Al (0.143 nm) is much larger than those of the other four elements (0.124-0.128 nm). Therefore, the fixed positioning of Al atoms in the BCC → B2 ordering transition greatly reduces the lattice distortion, resulting in the dramatic resistivity decrease of the HEA films observed in the second stage in Fig. 5. The disorder-order transition simultaneously causes the composition segregation. According to the mixing enthalpies between Al and the other four elements [44]:  $\Delta H_{\text{Al-Ni}} = -22 \text{ kJ/mol}, \Delta H_{\text{Al-Co}} = -19 \text{ kJ/mol}, \Delta H_{\text{Al-Fe}} = -11 \text{ kJ/mol}$ mol, and  $\Delta H_{\rm Al-Cr} = -10$  kJ/mol, Al atoms are more likely to attract Ni and Co atoms as neighbors, since the  $\Delta H_{\rm Al-Ni}$  and  $\Delta H_{\rm Al-Co}$  are more negative. Hence, the Al-rich B2 phase is also relatively rich in Ni and Co, and the remaining BCC phase after the ordering transition contains more Fe and Cr, which can be considered as the Fe- and Cr-rich BCC' phase.

In the bulk HEAs where the B2 phase already exists, the BCC' phase continues transforming into the  $\sigma$  phase (a disordered solid solution composed almost entirely of Fe and Cr [45,46]), along with the Ni- and Co-rich FCC phase during heating. This transition had been reported to occur at around 873 K in bulk Al, CoCrFeNi HEAs [33,45], which is consistent with the XRD results in this paper. In the transition of BCC'  $\rightarrow \sigma$  + FCC, because Cr diffuses faster than Co, Fe, and Ni in HEAs [47], the precipitation of the  $\sigma$  phase is accelerated in the Cr-segregation areas [48]. Simultaneously, the Ni- and Co-rich FCC phase is formed in the areas with the depleted Cr [33]. As mentioned above, except for Al atoms, the atomic radii of the other four elements are very similar, indicating that the segregation of Cr and Fe can hardly affect the lattice-distortion degree. Therefore, the sudden small resistivity increase at around 873 K of bulk HEAs in Fig. 5 corresponds to the transition of BCC'  $\rightarrow \sigma$  + FCC, and the resistivity only changed about 10 μ $\Omega$ ·cm.

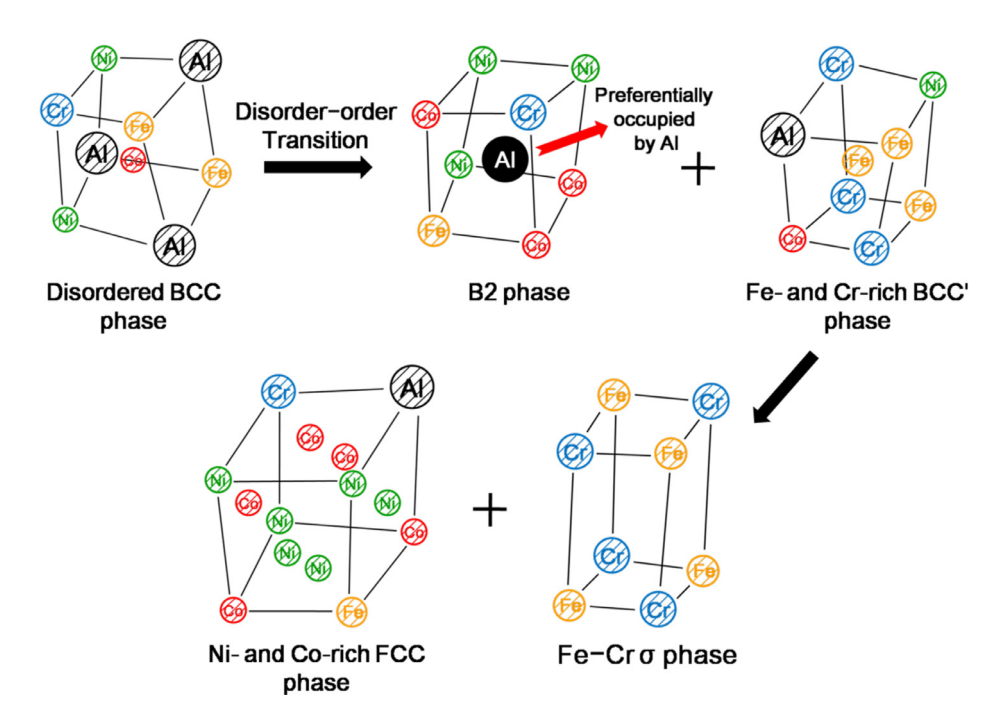


Fig. 8. Schematic of the BCC  $\rightarrow$  B2 and BCC'  $\rightarrow$   $\sigma$  + FCC phase transitions in the Al<sub>x</sub>CoCrFeNi HEAs during heating. Spheres with shadow-pattern represent positions randomly occupied by each element, and the solid sphere denotes the position preferentially occupied by Al atoms.

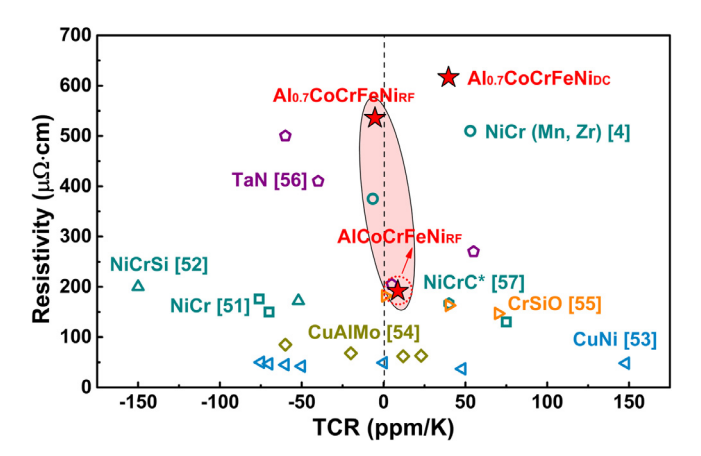


Fig. 9. TCRs and resistivity of the  $Al_x$ CoCrFeNi HEA films, compared with multiple types of thin-films prepared by magnetron sputtering [51–57]. The resistivity of NiCrC\* film was calculated from the sheet resistance and film thickness given in the literature [57].

In many disordered alloys, such as Fe – Al [49] and Fe – Co – V [50] alloys, as the temperature increases to the point that atom migration is appreciable, leading to the long-range ordering, the resistivity changes almost immediately when the ordering begins, and the ordering temperature in disordered alloys is lower than 573 K in general. This behavior is markedly different from the short-range ordering, which usually changes the resistivity in a certain temperature range [7]. The rapid resistivity decline of the Al $_{\rm x}$ CoCrFeNi HEA films at around 565 K further confirms that their resistivity – temperature properties belong to the category of disordered alloys.

#### 4.3. Application potential of Al<sub>x</sub>CoCrFeNi HEA films

Fig. 9 presents the TCRs and resistivity of the  $Al_x$ CoCrFeNi HEA films, compared with multiple types of thin-films prepared by magnetron sputtering [51–57]. To allow accurate comparisons, the RT resistivity of the HEA films was measured by the four-point probe tester. When calculating the TCRs of the HEA films, the temperature range is

from RT to 398 K, and the resistivity was measured by the thermal resistance tester.

For a certain kind of thin-films, no matter of metal alloys or cermets, it is hard to keep the TCRs low while expanding the resistivity range [1]. This trend is clearly showed in Fig. 9 for the TaN films [56] (200–500  $\mu\Omega$ ·cm) and the NiCr (Mn, Zr) films [4] (350–500  $\mu\Omega$ ·cm) with the relatively-large resistivity. As the resistivity of these films increased to around 500  $\mu\Omega$ -cm, the TCRs could not remain within  $\pm$ 50 ppm/K. Moreover, even without considering any kind of specific alloy system, the resistivity of a thin film still lies in a certain limited range if its TCR is near zero, as the relationship between the resistivity and TCRs of thin films reported by Mooij [6]. The summarized data from dozens of alloy systems reveal that when the resistivity of thin films increased from 20 to 300  $\mu\Omega\text{-cm},$  the TCRs changed from a large positive value (about 200 ppm/K) to a large negative value (about -200 ppm/K). However, for the thin films with TCRs near zero (within  $\pm$  50 ppm/K), their resistivity is only concentrated in the range of  $100-200 \,\mu\Omega$ ·cm.

Therefore, it is difficult for thin films to simultaneously possess low TCRs and a wide range of tunable resistivity. However, seen from the data of the HEA films in Fig. 9, the AlCoCrFeNi\_{RF} and Al\_{0.7}CoCrFeNi\_{RF} films both have TCRs within  $\pm$  10 ppm/K, but their resistivity is more than 300  $\mu\Omega$ -cm different. It shows that the Al\_xCoCrFeNi HEA films can still maintain low TCRs when their resistivity is modulated over a wide range. Especially, the Al\_0.7CoCrFeNi\_{RF} film simultaneously possesses high resistivity (535.9  $\mu\Omega$ -cm) and an ultralow TCR (-5 ppm/K), which is almost impossible to obtain for single-layer as-deposited thin films of conventional-alloy systems. From the perspective of the preparation process, the Al\_xCoCrFeNi HEA films only contain low-cost metal elements and the sputtering process is easy to control. In addition, the as-deposited HEA films already have low TCRs without annealing or other treatments, which can be another advantage for manufacturing thin-film resistors.

In summary, the current work provides a comparative study on the resistivity – temperature behavior of film and bulk  $Al_x$ CoCrFeNi HEAs with similar compositions. The HEA films with an ultralow TCR and widely-tunable resistivity are presented, exhibiting the advantages over conventional-alloy thin films. On this basis, the resistivity properties of

larger composition ranges of the  ${\rm Al}_x{\rm CoCrFeNi}$  HEAs and other HEA systems still need to be explored further. The concept of multi-element results in the highly-disordered characteristic of HEAs, stimulating more potential for their properties. Furthermore, it will certainly provide larger development spaces and more ideas for the field of thin-film resistive materials.

#### 5. Conclusions

In this paper, the resistivity-temperature behaviors of the Al<sub>x</sub>CoCrFeNi (x = 0.7.1) HEA films prepared by magnetron sputtering from RT to 1078 K are explained, and the differences of the behavior between film and bulk HEAs with similar compositions are analyzed. Main conclusions can be drawn as followed: The HEA films are composed of FCC and BCC phases nanocolumnar grains, which are more chemically disordered than that of the bulk  $Al_x$ CoCrFeNi (x = 0.74, 0.92) HEAs with mainly the BCC and B2 phases. The resistivity-temperature curves of the Al<sub>x</sub>CoCrFeNi film and bulk HEAs can be divided into two stages and the dividing points are 565 K and 723 K, respectively. In the first stage, the resistivity changed slowly with temperature, the correlation between high resistivity and small TCRs of the HEAs is in accord with the saturation effect. After considering multiple factors, including the s-d scattering effects, the resistivity–temperature curves of the  ${\rm Al_x}{\rm CoCrFeNi}$  HEAs can be described by the formula of  $\rho = b_0 + b_1 T(1 - b_2 T^2)$ . In the second stage, the resistivity shows an obvious change, for the HEA films, it decreased dramatically due to the formation of the B2 phase during the disorder-order transition, while for the bulk HEAs, the sudden small increase appeared at around 873 K, which corresponded to the transition of BCC'  $\rightarrow \sigma$  + FCC. The TCR of Al<sub>x</sub>CoCrFeNi HEA films maintain a low value while the resistivity is modulated over a wide range. Particularly, the Al<sub>0.7</sub>CoCrFeNi<sub>RF</sub> film simultaneously possesses high resistivity (535.9  $\mu\Omega$ ·cm) and an ultralow TCR (-5 ppm/K). The advantage of multi-elements of HEAs provides more potential and possibilities when pursuing comprehensive properties.

### CRediT authorship contribution statement

Chenyu Wang: Conceptualization, Methodology, Formal analysis, Investigation, Writing - original draft, Visualization. Xiaona Li: Conceptualization, Methodology, Validation, Writing - review & editing, Visualization. Zhumin Li: Formal analysis, Investigation, Writing - review & editing. Qing Wang: Methodology, Validation, Writing - review & editing, Visualization. Yuehong Zheng: Investigation, Writing - review & editing. Yue Ma: . Linxia Bi: . Yuanyuan Zhang: . Xihui Yuan: . Xin Zhang: Formal analysis, Investigation. Chuang Dong: Visualization, Writing - review & editing. Peter K. Liaw: Visualization, Writing - review & editing.

## **Declaration of Competing Interest**

The authors declare that they have no known competing financial interests or personal relationships that could have appeared to influence the work reported in this paper.

## Acknowledgements

We gratefully acknowledge the financial supports by the National Key Research and Development Program of China (grant no. 2017YFB0306100), the National Natural Science Foundation of China [U1867201], the Fundamental Research Funds for the Central Universities (grant no. DUT17LAB09), the Science Challenge Project (TZ2016004), &the National Science Foundation (DMR-1611180 and 1809640) with the program directors, Drs G. Shiflet and D. Farkas.

#### References

- C. Cherian Lukose, G. Zoppi, M. Birkett, Thin film resistive materials: past, present and future, IOP Conf. Series: Mater. Sci. Eng. 104 (2015) 012003.
- [2] L.F. Lai, X.S. Su, X.Z. Fu, R. Sun, C.P. Wong, The microstructure and properties of C and W co-doped NiCr embedded thin film resistors, Surf. Coat. Technol. 259 (2014) 759–766
- [3] D.W. Lee, Y.N. Kim, M.Y. Cho, P.J. Ko, D. Lee, S.M. Koo, K.S. Moon, J.M. Oh, Reliability and characteristics of magnetron sputter deposited tantalum nitride for thin film resistors, Thin Solid Films 660 (2018) 688–694.
- [4] C.H. Lin, H.Y. Lee, Y.T. Tseng, Y.C. Lee, A study on the NiCrMnZr thin film resistors prepared using the magnetron sputtering technique, Thin Solid Films 660 (2018) 695–704
- [5] D.B. Miracle, O.N. Senkov, A critical review of high entropy alloys and related concepts, Acta Mater. 122 (2017) 448–511.
- [6] J.H. Mooij, Electrical conduction in concentrated disordered transition metal alloys, Physica Status Solidi 17 (1973) 521–530.
- [7] C.D. Starr, Correlation of electrical conductivity and resistivity of solid solution alloys with temperature coefficient of resistance, Trans. Metallurg. Soc. AIME 227 (1963) 60–64.
- [8] S.M. Na, I.S. Park, S.Y. Park, G.H. Jeong, S.J. Suh, Electrical and structural properties of Ta–N thin film and Ta/Ta–N multilayer for embedded resistor, Thin Solid Films 516 (2008) 5465–5469.
- [9] H.J. Kim, J.S. Song, I.S. Kim, S.S. Kim, Electrical characteristics of Ti–O/Ta<sub>2</sub>O<sub>5</sub> thin film sputtered on Ta/Ti/AL<sub>2</sub>O<sub>3</sub> substrate, Thin Solid Films 446 (2004) 124–127.
- [10] N.G. Galkin, T.V. Velitchko, S.V. Skripka, A.B. Khrustalev, Semiconducting and structural properties of CrSi<sub>2</sub>, A-type epitaxial films on Si(111), Thin Solid Films 311 (1997) 230–238.
- [11] X.Y. Wang, Z.S. Zhang, T. Bai, Investigation on powder metallurgy Cr–Si–Ta–Al alloy target for high-resistance thin film resistors with low temperature coefficient of resistance, Mater. Des. 31 (2010) 1302–1307.
- [12] J.W. Yeh, S.K. Chen, S.J. Lin, J.Y. Gan, T.S. Chin, T.T. Shun, C.H. Tsau, S.Y. Chang, Nanostructured high-entropy alloys with multiple principal elements: novel alloy design concepts and outcomes, Adv. Eng. Mater. 6 (2004) 299–303.
- [13] Y. Zhang, T.T. Zuo, Z. Tang, M.C. Gao, K.A. Dahmen, P.K. Liaw, Z.P. Lu, Microstructures and properties of high-entropy alloys, Prog. Mater. Sci. 61 (2014) 1–93
- [14] J.W. Yeh, S.J. Lin, T.S. Chin, J.Y. Gan, S.K. Chen, T.T. Shun, C.H. Tsau, S.Y. Chang, Formation of simple crystal structures in Cu–Co–Ni–Cr–Al–Fe–Ti–V alloys with multiprincipal metallic elements, Metallurg. Mater. Trans. A35 (2004) 2533–2536.
- [15] H.P. Chou, S.Y. Chang, S.K. Chen, J.W. Yeh, Microstructure, thermophysical and electrical properties in AlxCoCrFeNi (0 ≤ x ≤ 2) high-entropy alloys, Mater. Sci. Eng. B163 (2009) 184–189.
- [16] Y.F. Kao, S.K. Chen, T.J. Chen, P.C. Chu, J.W. Yeh, S.J. Lin, magnetic Electrical, and hall properties of AlxCoCrFeNi high-entropy alloys, J. Alloys Compounds 509 (2011) 1607–1614.
- [17] S.K. Chen, Y.F. Kao, Near-constant resistivity in 4.2-360 K in B2 Al2.08CoCrFeNi, AIP Adv. 2 (2012) 012111.
- [18] S. Shafeie, S. Guo, Q. Hu, H. Fahlquist, P. Erhart, A. Palmqvist, High-entropy alloys as high-temperature thermoelectric materials, J. Appl. Phys. 118 (2015) 184905.
- [19] S. Shafeie, S. Guo, P. Erhart, Q. Hu, A. Palmqvist, Balancing scattering channels: a panoscopic approach toward zero temperature coefficient of resistance using highentropy alloys, Adv. Mater.20181805392.
- [20] J.W. Yeh, Physical metallurgy, in: M.C. Gao, J.W. Yeh, P.K. Liaw, Y. Zhang (Eds.), High-entropy alloys: Fundamental applications, Springer, 2016, pp. 51–113.
   [21] C.W. Tsai, S.W. Lai, K.H. Cheng, M.H. Tsai, A. Davison, C.H. Tsau, J.W. Yeh, Strong
- [21] C.W. Tsai, S.W. Lai, K.H. Cheng, M.H. Tsai, A. Davison, C.H. Tsau, J.W. Yeh, Strong amorphization of high-entropy AlBCrSiTi nitride film, Thin Solid Films 520 (2012) 2613–2618.
- [22] S.I. Vorobiov, D.M. Kondrakhova, S.A. Nepijko, D.V. Poduremne, N.I. Shumakova, I.Y. Protsenko, Crystalline structure, electrophysical and magnetoresistive properties of high entropy film alloys, J. Nano Electron. Phys. 8 (2016) 03026.
- [23] C.Y. Cheng, J.W. Yeh, High-entropy BNbTaTiZr thin film with excellent thermal stability of amorphous structure and its electrical properties, Mater. Lett. 185 (2016) 456–459.
- [24] R.C. Lin, T.K. Lee, D.H. Wu, Y.C. Lee, A study of thin film resistors prepared using Ni–Cr–Si–Al–Ta high entropy alloy, Adv. Mater. Sci. Eng. 2015 (2015) 847191.
- [25] W.J. Chen, T.Y. Liu, H.Y. Lee, Y.C. Lee, Ni–Cr–Mn–Y–Nb resistive thin film prepared by co-sputtering, Mater. Chem. Phys. 210 (2017) 327–335.
- [26] W. Li, P. Liu, P.K. Liaw, Microstructures and properties of high-entropy alloy films and coatings: a review, Mater. Res. Lett. 6 (2018) 199–229.
- [27] X.B. Feng, W. Fu, J.Y. Zhang, J.T. Zhao, J. Li, K. Wu, G. Liu, J. Sun, Effects of nanotwins on the mechanical properties of AlxCoCrFeNi high entropy alloy thin films, Scr. Mater. 139 (2017) 71–76.
- [28] W.B. Liao, S. Lan, L.B. Gao, H.T. Zhang, S. Xu, J. Song, X.L. Wang, Y. Lu, Nanocrystalline high-entropy alloy (CoCrFeNiAl0.3) thin-film coating by magnetron sputtering, Thin Solid Film 638 (2017) 383–388.
- [29] W.B. Liao, H.T. Zhang, Z.Y. Liu, P.F. Li, J.J. Huang, C.Y. Yu, Y. Lu, High strength and deformation mechanisms of Al0.3CoCrFeNi high-entropy alloy thin films fabricated by magnetron sputtering, Entropy 21 (2019) 146.
- [30] Y.F. Kao, T.J. Chen, S.K. Chen, J.W. Yeh, Microstructure and mechanical property of as-cast, -homogenized, and -deformed AlxCoCrFeNi  $(0 \le x \le 2)$  high-entropy alloys, J. Alloys Compounds 488 (2009) 57–64.
- [31] C. Li, J.C. Li, M. Zhao, Q. Jiang, Effect of aluminum contents on microstructure and properties of AlxCoCrFeNi alloys, J. Alloys Compounds 504 (2010) S515–S518.
- [32] W.R. Wang, W.L. Wang, S.C. Wang, Y.C. Tsai, C.H. Lai, J.W. Yeh, Effects of al

- addition on the microstructure and mechanical property of AlxCoCrFeNi high-entropy alloys, Intermetallics 26 (2012) 44–51.
- [33] W.R. Wang, W.L. Wang, J.W. Yeh, Phases, microstructure and mechanical properties of AlxCoCrFeNi high-entropy alloys at elevated temperatures, J. Alloys Compounds 589 (2014) 143–152.
- [34] D.M. King, S.C. Middleburgh, L. Edwards, G.R. Lumpkin, M. Cortie, Predicting the crystal structure and phase transitions in high-entropy alloys, JOM 67 (2015) 2375–2380
- [35] Y. Ma, B.B. Jiang, C.L. Li, Q. Wang, C. Dong, P.K. Liaw, F. Xu, L.X. Sun, The BCC/B2 morphologies in AlxCoCrFeCr high-entropy alloys, Metals (Basel) 7 (2017) 57.
- [36] Y.P. Wang, B.S. Li, H.Z. Fu, Solid solution or intermetallics in a high-entropy alloy, Adv. Eng. Mater. 11 (2010) 641–644.
- [37] J. Alami, S. Bolz, K. Sarakinos, High power pulsed magnetron sputtering: fundamentals and applications, J. Alloys Compd. 483 (2009) 530–534.
- [38] R. Cremer, M. Witthaut, D. Neuschütz, T.Leyendecker G.Erkens, M. Feldhege, Comparative characterization of alumina coatings deposited by RF, DC and pulsed reactive magnetron sputtering, Surf. Coat. Technol. 120-121 (1999) 213–218.
- [39] S. Tan, X.H. Zhang, X.J. Wu, F. Fang, J.Q. Jiang, Comparison of chromium nitride coatings deposited by DC and RF magnetron sputtering, Thin Solid Films 519 (2011) 2116–2120.
- [40] T.T. Shun, C.H. Hung, C.F. Lee, The effects of secondary elemental Mo or Ti addition in Al0.3CoCrFeNi high-entropy alloy on age hardening at 700 °C, J. Alloys Compounds 495 (2010) 55–58.
- [41] L.V. Meisel, P.J. Cote, Structure factors in amorphous and disordered harmonic Debye solids, Phys. Rev. B Condens. Matter. 16 (1977) 2978–2980.
- [42] P.J. Cote, L.V. Meisel, Origin of saturation effects in electron transport, Phys. Rev. Lett. 40 (1978) 1586–1589.
- [43] N.F. Mott, Electrons in transition metals, Adv. Phys. 13 (1964) 325-422.
- [44] A.I. Takeuchi, Classification of bulk metallic glasses by atomic size difference, heat of mixing and period of constituent elements and its application to characterization of the main alloying element, Mater. Trans. 46 (2005) 2817–2829.
- [45] M.H. Tsai, K.C. Chang, J.H. Li, R.C. Tsai, A.H. Cheng, A second criterion for sigma phase formation in high-entropy alloys, Mater. Res. Lett. 4 (2016) 1–6.

- [46] J.M. Hao, Y. Ma, Q. Wang, C. Zhang, C.L. Li, C. Dong, Q. Song, P.K. Liaw, Formation of cuboidal B2 nanoprecipitates and microstructural evolution in the body-centered-cubic Al0.7NiCoFe1.5Cr1.5 high-entropy alloy, J. Alloys Compd. 780 (2019) 408–421.
- [47] K.Y. Tsai, M.H. Tsai, J.W. Yeh, Sluggish diffusion in Co-Cr-Fe-Mn-Ni high-entropy alloys, Acta Mater. 61 (2013) 4887–4897.
- [48] C.C. Hsieh, W. Wu, Overview of intermetallic sigma (o) phase precipitation in stainless steels, Int. Sch. Res. Notices 2012 (2013) 1–16.
- [49] G.A. Thomas, A.B. Giray, R.D. Parks, Critical resistivity near an order-disorder transition, Phys. Rev. Lett. 31 (1973) 241–244.
- [50] S. Hasani, A. Shafyei, M. Nezakat, H. Mostaan, P. Behjati, P. Sahu, The effect of the order-disorder transition on the electrical, magnetic and mechanical properties of vicalloy i, Intermetallics 81 (2017) 73–79.
- [51] S. Vinayak, H.P. Vyas, V.D. Vankar, Microstructure and electrical characteristics of Ni–Cr thin films, Thin Solid Films 515 (2007) 7109–7116.
- [52] H.Y. Cheng, Y.C. Chen, P.J. Li, C.F. Yang, H.H. Huang, Effect of annealing process on the properties of Ni(55%)Cr(40%)Si(5%) thin-film resistors, Materials (Basel) 8 (2015) 6752–6760.
- [53] J.J.V.D. Broek, J.J.T.M. Donkers, R.A.F.V.D. Rijt, J.T.M. Janssen, Metal film precision resistors: resistive metal films and a new resistor concept, Philips J. Res. 51 (1998) 429–447.
- [54] M. Birkett, J. Brooker, R. Penlington, A. Wilson, Electrical characterisation of AlCuMo thin films prepared by dc magnetron sputtering, IET Sci. Meas. Technol. 2 (2007) 304–309
- [55] R. Glang, R.A. Holmwood, S.R. Herd, Resistivity and structure of Cr–SiO cermet films, J. Vacuum Sci. Technol. 4 (1967) 163–170.
- [56] C.M. Wang, J.H. Hsieh, C. Li, Y. Fu, T.P. Chen, Effects of annealing on the microstructure and electrical properties of TaN–Cu nanocomposite thin films, Surf. Coat. Technol. 193 (2005) 173–177.
- [57] L. Lai, J. Wang, H. Wang, M. Bao, Structures and properties of C-doped NiCr thin film deposited by closed-field unbalanced magnetron sputtering, J. Electron. Mater. 46 (2017) 1–11.